EARTH SURFACE PROCESSES AND LANDFORMS
Earth Surf. Process. Landforms (2008)

Published online in Wiley InterScience
(www.interscience.wiley.com) DOI: 10.1002/esp.1768

Assessing the effect of vegetation-related bank strength on channel morphology and stability in gravel-bed streams using numerical models

Brett C. Eaton[1]* and Tim R. Giles[2]
[1] Geography Department, The University of British Columbia, Vancouver, British Columbia, Canada
[2] B.C. Ministry of Forests and Range, Kamloops, British Columbia, Canada

Received 12 June 2008; Revised 9 September 2008; Accepted 16 October 2008

* Correspondence to: Brett C. Eaton, Geography Department, The University of British Columbia, Vancouver, British Columbia, V6T 1Z2, Canada. E-mail brett.eaton@ubc.ca

ESPL
Earth Surface Processes and Landforms

ABSTRACT: Bank strength due to vegetation dominates the geometry of small stream channels, but has virtually no effect on the geometry of larger ones. The dependence of bank strength on channel scale affects the form of downstream hydraulic geometry relations and the meandering-braiding threshold. It is also associated with a lateral migration threshold discharge, below which channels do not migrate appreciably across their floodplains. A rational regime model is used to explore these scale effects: it parameterizes vegetation-related bank strength using a dimensionless effective cohesion, C_r^*. The scale effects are explored primarily using an alluvial state space defined by the dimensionless formative discharge, Q^*, and channel slope, S, which is analogous to the Q–S diagrams originally used to explore meandering-braiding thresholds. The analyses show that the effect of vegetation on both downstream hydraulic geometry and the meandering-braiding threshold is strongest for the smallest streams in a watershed, but that the effect disappears for $Q^* > 10^6$. The analysis of the migration threshold suggests that the critical discharge ranges from about 5 m^3/s to 50 m^3/s, depending on the characteristic rooting depth for the vegetation. The analysis also suggests that, where fires frequently affect riparian forests, channels may alternate between laterally stable gravel plane-bed channels and laterally active riffle-pool channels. These channels likely do not exhibit the classic dynamic equilibrium associated with alluvial streams, but instead exhibit a cyclical morphologic evolution, oscillating between laterally stable and laterally unstable end-members with a frequency determined by the forest fire recurrence interval. Copyright © 2008 John Wiley & Sons, Ltd.

KEYWORDS: vegetation-related bank strength; channel morphology; channel stability; gravel-bed streams; numerical models

Introduction

The dynamics and morphology of a stream are affected by the nature of the channel boundary (e.g. Andrews, 1982; Huang and Nanson, 1998; Rowntree and Dollar, 1999). In particular, the ability of the stream to erode its banks is arguably critical for the establishment and maintenance of meandering channels (Friedkin, 1945), braided channels (Carson, 1984; Simpson and Smith, 2001) and anabranched channels (Nanson and Knighton, 1996). Bank vegetation, in particular, seems to be an important component of the channel boundary (Hickin, 1984; Friedman *et al.*, 1996; Hupp and Osterkamp, 1996; Abernethy and Rutherfurd, 1998; Millar, 2000; Gran and Paola, 2001; Simon and Collison, 2002; Brooks *et al.*, 2003; Jeffries *et al.*, 2003; Murray and Paola, 2003; Tal *et al.*, 2004; Gaeuman *et al.*, 2005; Pollen and Simon, 2005; Tal and Paola, 2007). The recent development of several models for assessing the effect of vegetation on bank stability attest to the importance of this line of research (Van de Wiel and Darby, 2007; Pollen-Bankhead, and Simon, 2008). Bed texture is another important boundary condition that determines channel dynamics (Dietrich *et al.*, 1989; Church *et al.*, 1998; Tribe and Church, 1999; Church and Hassan, 2002; Lisle and Church, 2002; Church, 2006). However, with some notable exceptions (Andrews, 1984; Hey and Thorne, 1986; Dade, 2000; Pitlick and Cress, 2002; Millar, 2005), these boundary conditions are not included in the sorts of scaling relations – such as downstream hydraulic geometry equations and models describing the meandering-braiding transition – that are often used to predict channel change (e.g. Church, 1995) and landscape evolution (e.g. Tucker and Bras, 1998).

The characteristics of the surface of a gravel-bed stream (primarily the bed texture and nature and abundance of surface structures) develop in response to the fluid and sediment flux supplied to the stream channel (Parker and Klingeman, 1982; Reid *et al.*, 1992; Wilcock and McArdell, 1993) and can mediate the sediment transport rate (Dietrich *et al.*, 1989; Buffington and Montgomery, 1999). The effects of bed surface can be incorporated into an analysis of the general scaling functions in fluvial geomorphology by using non-dimensional parameters, such as dimensionless depth, width and discharge (Parker, 1979; Andrews, 1984; Pitlick and Cress, 2002; Millar, 2005) or the dimensionless shear stress to describe the system (Eaton *et al.*, 2004; Church, 2006).

The inclusion of the effect of bank strength due to vegetation is rather more difficult. In some streams, bank strength is

attributable to non-alluvial boundaries such as bedrock, over-consolidated glacial deposits or human structures, with the result that the channel boundaries may be effectively fixed in place over regime timescales (Church, 2006). Bank strength due to cohesion in fine over-bank deposits is also common, particularly in larger river systems with fine bed material. The rate of bank migration in these systems may be exceedingly slow (e.g. Brooks, 2003) and again the banks may be effectively fixed over regime timescales. Bank strength is also affected by riparian vegetation (Andrews, 1982; Hey and Thorne, 1986): this form of bank strength is scale dependent, declining as the size of the stream channel under consideration increases (Eaton and Millar, 2004; Eaton and Church, 2007).

Rational regime theories relate reach-average hydraulic conditions, in conjunction with a sediment transport law and equations describing bank stability, to the stable channel geometry, thereby directly linking channel morphology to the formative discharge and the long-term average sediment supply. They are ideally suited to the study of the interaction between boundary conditions, including surface texture and riparian vegetation type, and channel geometry. Various regime models have been constructed that explicitly parameterize the effect of riparian vegetation (Millar and Quick, 1993; Eaton, 2006) and cohesive sediment (Millar and Quick, 1998) on bank strength. A more general form of regime theory that simply expresses bank strength relative to the bed has also been developed, and was used to generate simple power functions that approximate the predictions of the complete regime model by invoking reasonable assumptions about the relation between flow resistance, boundary properties (such as the friction angle) and the median surface grain size (D_{50}) of the stream (Millar, 2005). All regime models that explicitly consider bank strength are solved numerically and require some sort of optimality criterion to select a unique solution from a range of potential solutions (e.g. Kirkby, 1977; Chang, 1979; White *et al.*, 1982; Davies and Sutherland, 1983; Huang *et al.*, 2004). An optimality criterion can be thought of a mathematical formalism that adapts a one-dimensional (1D) numerical model (i.e. regime theory) to the description of a three-dimensional (3D) reality by encapsulating some underlying process that cannot be explicitly represented in the numerical model. For example, Eaton *et al.* (2006) present a conceptual model that relates the flow resistance-based optimality criterion proposed by Eaton *et al.* (2004) to the onset of meandering by considering the stability of cross-stream distribution of shear stress and sediment transport field, in which case the tendency to meander is the underlying process not considered by the model. Experimental tests of Eaton *et al.*'s optimality criterion demonstrate that the trajectories by which channel stability is established are consistent with the theory (Eaton *et al.*, 2004).

Since regime theory is physically based, regime models are also suitable for investigating the influence of grain size. In this paper, two formulations of regime theory are used to investigate how grain size and bank strength due to vegetation affect downstream hydraulic geometry relations, the braiding-meandering threshold and the threshold for lateral migration described by Beechie *et al.* (2006): (1) a general form of regime theory, expressed using the dimensionless equations reported by Millar (2005); (2) a more specific model that applies to vegetated gravel-bed rivers (Eaton, 2006).

Methods

There are three scale-related issues that are investigated in this paper: (1) the potential for downstream hydraulic geometry to be influenced by systematic (but typically unrecognized) changes in relative bank strength with channel scale, even when differences in riparian vegetation and characteristic grain size are accounted for; (2) the effect of vegetation on the meandering-braiding transition; (3) the effect of vegetation on the ability of a channel to migrate laterally across its floodplain. All three issues are investigated by comparing previously published results with predictions from our two formulations of rational regime theory.

In part of our analysis, we use the dimensionless hydraulic geometry equations presented by Millar (2005) to predict channel geometry. These equations represent a general form of regime theory in which bank strength is expressed relative to the bed (referred to as the relative bank strength, μ'): for clarity, these will be referred to in this paper as the Constant Relative Bank (CRB) strength equations.

In the remainder of our analysis, we use a regime model employing the bank stability approach proposed by Eaton (2006) to predict channel geometry, which applies to gravel-bed rivers with vegetated floodplains. In this model, bank strength is described primarily by an effective cohesion that is attributed to the root system of the riparian vegetation (C_r): for the sake of clarity, this is referred to as the CCV model (for Constant effective Cohesion due to Vegetation). An Excel version of the CCV model and a user's manual describing the input variables and the operation of the program are available from the *Earth Surface Processes and Landforms* journal website. The Excel file also includes an interface for calculating channel geometry using Millar's (2005) CRB equations.

CRB equations

Millar (2005) uses a rational regime model to define dimensionless hydraulic geometry equations that depend on the dimensionless discharge, Q^*, channel slope, S, and relative bank strength, μ', all of which are dimensionless constants. The variable Q^* is defined by the equation:

$$Q^* = \frac{Q}{\sqrt{(s-1)gD_{50}}\,D_{50}^2} \tag{1}$$

where Q is the formative discharge (in m^3/s), s is the relative density of the sediment grains (2·65), g is the acceleration of gravity (9·8 m/s^2) and D_{50} is the surface median grain size (in mm). Q^* is an expression of the scale of the system that accounts for variations both discharge and grain size.

The parameter, μ', is the ratio of the force required to erode the banks to that required to erode the bed ($\mu' = \tau_{c(bank)}/\tau_{c(bed)}$, where τ_c is the critical shear stress for entrainment of either the bed or the banks). When the bed and banks are composed of identical materials and the floodplain is not vegetated, μ' is unity; for small, densely forested streams where root systems may permeate nearly the entire channel bank, μ' can be as high as 20 (Eaton and Church, 2007). The parameter μ' can be shown to be mathematically identical to the modified friction angle (ϕ') proposed by Millar and Quick (1993) and used by Eaton *et al.* (2004).

Millar's (2005) physically based hydraulic geometry equations, referred to herein as the CRB equations, are:

$$W^* = 16{\cdot}5Q^{*0{\cdot}70}\,S^{0{\cdot}60}\mu'^{-1{\cdot}10} \tag{2}$$

$$d^* = 0{\cdot}125Q^{*0{\cdot}16}\,S^{-0{\cdot}62}\mu'^{0{\cdot}64} \tag{3}$$

where W^* is the dimensionless width (W/D_{50}) and d^* is the dimensionless depth (d/D_{50}). These equations were derived

DOI: 10.1002/esp

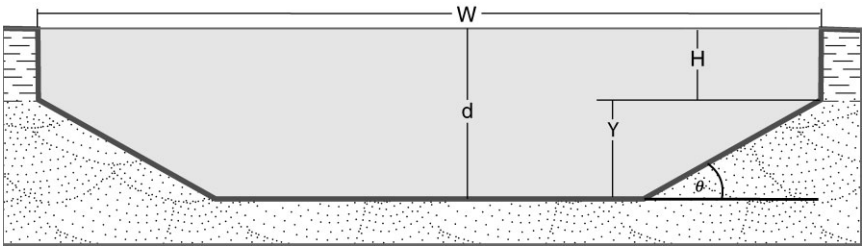

Figure 1. Cross-sectional geometry for the regime model of Eaton (2006). The upper, vertical bank section (H) is associated with over bank and bar top deposition of suspended sediments, combined with colonization by vegetation. The lower bank section (having thickness, Y and average gradient, θ) represents the cohesionless bedload deposited in channel bars. The total depth (d) and width (W) are numerically solved by the CCV model.

statistically from a large number of regime model predictions using the μ' parameterization of bank strength. We know from previous work (Eaton *et al.*, 2004) that the W/d ratio is constant for unique values of μ' and dimensionless shear stress (τ^*), regardless of the actual magnitude of the formative discharge. Therefore the effect μ' on the channel geometry is independent of channel scale.

CCV model

The CCV model is a numerical rational regime model that expresses bank strength using two parameters (see Figure 1): (1) a friction angle, ϕ, that characterizes the frictional resistance of the sediment found in the lower part of the channel bank; and (2) a root cohesion term, C_r, that characterizes the stabilizing effect of vegetation on the upper bank (Eaton, 2006). While friction angle does vary slightly with particle size and angularity, ϕ is held constant for all of the runs herein, since it does not vary with vegetation type. As noted by Eaton (2006), this bank stability approach is strictly valid only for gravel-bed streams with a cohesionless lower bank composed primarily of bedload accumulated in channel bars and an upper bank dominated by the strength imparted by riparian root systems, which will often be composed of suspended sediment deposits (primarily cohesionless sand and silt). This bank sedimentology is common for laterally active gravel-bed streams.

For the CCV model, the solution channel geometry is found by numerically varying the width of the channel, along with the thickness of the lower bank section (Y) and the angle of the lower bank (θ) to find all channels that have stable banks, then applying Eaton *et al.*'s (2004) optimality criterion to select the most stable (hence probable) channel state. The upper bank height, H is determined by the selected value of C_r and is thus constant.

Just as true cohesion is directly related to the maximum possible stable bank height for a vertical cut into a cohesive deposit, the cohesion due to riparian root systems (C_r) can be related to the maximum stable vertical bank height, H. Eaton (2006) showed that, for fully saturated channel banks, the relation between H and C_r is given by:

$$H = \frac{2C_r}{\gamma_b \cos\alpha}\left(\frac{1}{\sin\alpha - (\cos\alpha - \gamma/\gamma_b)\tan\phi_u}\right) \qquad (4)$$

where: φ_u is the friction angle for the upper bank material; $\alpha = 45 + \varphi_u/2$, following Carson and Kirkby, (1972, p. 116); γ_b is the bulk unit weight for the upper bank; and γ is the unit weight of water. Since α, φ_u, γ_b, and γ are effectively constant, it is clear that H and C_r are linearly related to one another.

In Eaton's (2006) derivation of Equation 4, the stability of the upper bank is assessed assuming that the bank will fail via a slab failure, which provides a minimum estimate of the root cohesion, C_r, since the height of the upper banks observed in the stream may be equal to or less than the critical H predicted by Equation 4. From the point-of-view of the model, this is irrelevant, since the numerical analysis performed in the CCV model uses H as a (constant) boundary condition, and the stability analysis is performed on the lower bank on the understanding that, in general, erosion of the bank toe is usually responsible for bank retreat. If the rooting depth is shallow but the root cohesion is very high, then the banks can be undercut and thence fail by toppling or cantilever failure: the reach-average widths in this case will likely be the same as it would for a system with the same rooting depth but lower root cohesion. Therefore, the most direct way of parameterizing the effect of vegetation on bank strength is by directly specifying a value of H, which is interpreted as the rooting depth for the riparian vegetation, realizing that – given a series of assumptions about the mode of bank failure – H is directly proportional to an average root cohesion value for the upper bank, C_r. Thinking more specifically about what controls the thickness of the upper bank layer shown in Figure 1, it is reasonable to speculate that H is related to the deposition of the upper bank sediments, which often occurs in concert with vegetation colonization, since a vegetative cover both promotes sedimentation and stabilizes the deposited material. Obviously, the effect of vegetation on bank strength is exceedingly difficult to parameterize, but the relative success of the analysis presented by Eaton (2006) and Eaton and Church (2007) suggests that this approach is relatively robust.

Since the effect of vegetation in the CCV model is parameterized using H, the relative importance of vegetation-related bank strength depends on the ratio between H and the total channel depth, d. As one moves downstream, d increases while H presumably does not (assuming that the vegetation type does not also change) and thus the relative influence of riparian vegetation on bank strength declines. Since H has the units of length, it can be expressed non-dimensionally using the ratio H/D_{50}, which is defined here as the dimensionless effective cohesion due to vegetation (C_r^*), the relation between H and C_r being expressed in Equation 4.

Downstream hydraulic geometry relations

In order to assess the degree to which downstream hydraulic geometry equations reflect the scale-dependent effect of vegetation on bank strength, it is necessary to compare theory and field data. This has been done previously by comparing channel widths observed in the field with the widths predicted by regime theory (Eaton *et al.*, 2004; Eaton, 2006; Eaton and Church, 2007), but the systematic variations in relative bank strength that occur are not obvious in this sort of analysis. In order to explicitly reveal the scale-effect, we wish to test regime theory more generally. This is accomplished

DOI: 10.1002/esp

by determining the slope required in a regime model to reproduce the hydraulic geometry observed in the field, and then comparing the predicted slopes to those observed in the field. The comparison is conducted using Q^*–S plots, where S is the channel slope. This is similar to the Q–S diagrams used by Leopold and Wolman (1957) and others to investigate the meandering-braiding transition. Since S is not an independent variable in the traditional empirical hydraulic geometry equations of the form $W = aQ^b$, $d = cQ^f$ a comparison of the Q^*–S curves from a regime model fit to observed channel dimensions with the values of S observed in the field is still an independent test. The Q^*–S diagram is effectively a reduced form of the dimensionless alluvial state space proposed by Eaton *et al*. (2004).

The CCV model is used primarily to test the theory against the data and to reveal the underlying scaling relations. Using the CCV model, curves for the same value of C_r^* but with different D_{50} and H values collapse one on top of the other in Q^*–S space, but are clearly different in Q–S space: this is the main reason that C_r^* is used as a measure of bank strength in preference to H or C_r. While C_r^* is dimensionless, the effect that it has on the resulting channel geometry is dependent on the channel size (namely the channel depth), so the notion that the effect of a given vegetation type and density ought to decline as the size of the channel under consideration increases is preserved.

In our first analysis of the effects of vegetation-related bank strength on downstream hydraulic geometry, we use a previously published analysis by Eaton and Church (2007) of Emmett's (1975) data from the Salmon River area, Idaho. These stream channels are relatively small (Q varies from about 2 m^3/s to 150 m^3/s) with moderately dense riparian vegetation adjacent to them: they are divided into two groups, corresponding to two sub-basins of the Salmon River with different dominant bedrock types. The D_{50} for both groups varies from about 15 mm to 50 mm (for details, see Eaton and Church, 2007). In Eaton and Church's analysis, the value of H was first estimated based on the typical riparian vegetation found in the two basins, using Eaton's (2006) results as a reference, then the value of H was varied in order to reproduce the observed channel geometry. The data appear to be consistent with the CCV model assuming $H = 0{\cdot}45$ m for Group 1 and $H = 0{\cdot}70$ m for Group 2: according to Equation 4, these values correspond to root cohesion values, C_r, of about 1·9 kPa and 3·0 kPa, respectively, and to dimensionless effective cohesions, C_r^*, of about 13 and 20, respectively.

We compare the Q^*–S curves from the fitted CCV model against similar curves based on the CRB equations in which relative bank strength is assumed to be constant. In order to isolate the Q^*–S curves predicted by the CRB equations, we set Equation 2 equal to an empirically determined hydraulic geometry equation of the form $W^* = aQ^{*b}$ to determine the functional relation between S and Q^* associated with the reported hydraulic geometries. The empirical hydraulic geometry equation for the dataset was estimated by fitting a power function to the (dimensionless) widths and discharges for both groups of data, combined. Either the width or the depth equations can be used to solve to the Q^*–S function using the CRB equations, and both produce very similar results.

In our second analysis, we examine the hydraulic geometry data presented by Andrews (1984). The Andrews dataset classifies the field sites as having either 'thick' or 'thin' riparian vegetation, and the field sites span a wide range of Q^* values. The average D_{50} for these streams is 60 mm. In order to determine the Q^*–S scaling associated with the CRB equations, we followed the same procedure described earlier, in which a power function was fit using the dimensionless widths and discharges. To produce a Q^*–S relation for the CCV model, the parameter S was varied until the model reproduced the expected hydraulic geometry. Two values of C_r^* were modeled (1·67 and 3·33), both of which represent fairly low vegetation related bank strength. The resulting Q^*–S curves are compared to the analogous curves based on the CRB equations and to the actual field data.

In the third analysis of downstream hydraulic geometry, the CRB equations are used to generate a Q^*–S curve consistent with the empirical hydraulic geometry reported by Pitlick and Cress (2002). The CCV model is also used to numerically define a Q^*–S threshold for two values of dimensionless effective cohesion, C_r^* (13 and 4·4). Pitlick and Cress's data comes from the Colorado River in western Colorado and eastern Utah, representing relatively large channel types. The average surface D_{50} for the Colorado River in the study reach is about 45 mm. Analysis of this dataset by Eaton and Church (2007) indicates that the relative bank strength for all of the channels remains nearly constant because of their large size. In this case, vegetation should have very little effect on relative bank strength and on the channel geometry.

Meandering-braiding transition

The second scaling issue considered in this paper is the meandering-braiding transition. Bank strength in general and vegetation in particular plays an important role in determining the channel pattern for a river (Carson, 1984; Millar, 2000, 2005; Simpson and Smith, 2001). The CCV model is used to numerically determine the channel geometry at the meandering-braiding threshold for a range of D_{50}, H and Q values. For the sake of simplicity, the threshold is assumed to correspond to a W/d ratio of approximately 50, after Fredsoe (1978). The model output is used to illustrate the sensitivity of the threshold to the value of D_{50} and to H. It is also used to demonstrate how the threshold collapses onto a single Q^*–S curve for constant values of the dimensionless effective cohesion, C_r^*. Finally, the dimensionless Q^*–S thresholds for a range of C_r^* value are compared against data from braided channels and vegetated meandering channels.

Channel migration threshold

The last issue considered is the threshold for lateral activity. Based on a detailed analysis of historical aerial photographs, Beechie *et al*. (2006) identified a threshold for streams in the Pacific Northwest, below which channels do not appear to be able to migrate laterally. That threshold is reported to correspond to a discharge of about 15 m^3/s or a bankfull width of about 15–20 m. Furthermore, Beechie *et al*. (2006) argued that the threshold was associated with the rooting depths similar to the channel depth, which were thought to prevent the bank undercutting. The CCV model is used to identify the point at which the predicted channel depth is just 5% greater than H, where H is interpreted as a proxy for the rooting depth. This condition is easily predicted using numerical simulations invoking the CCV model because all of the quantities in Figure 1 remain defined (which is not the case when $H = d$). The simulations are run for various values of H, and the results are used to describe the channel migration threshold as a function of rooting depth. The CCV model was parameterized by imposing two constant values of D_{50} (30 mm and 45 mm) while holding Manning's n constant (0·06). It was also assumed that channel slope declines approximately in proportion to the square root of discharge. The precise slope–discharge relation

DOI: 10.1002/esp

used to parameterize the model ($S = 0{\cdot}0707Q^{-0{\cdot}55}$) was derived empirically from Emmett's (1975) dataset, analyzed by Eaton and Church (2007), but it is representative of the channels reported by Beechie *et al*. (2006).

The analysis of the lateral migration threshold is compared to the empirical observations made by Beechie *et al*. (2006). It is also applied to Fishtrap Creek, a small stream in the interior region of British Columbia where forest fire appears to have provoked rapid lateral migration following a period of lateral stability. The floodplain was affected by a forest fire in 2003, and nearly all of the trees on the floodplain died (Owens *et al*., 2006; Petticrew *et al*., 2006). There is a Water Survey of Canada hydrometric gauge in the study reach, continuously recording the stream discharge. Several monumented cross sections were established immediately after the fire.

Results

Downstream hydraulic geometry

Figure 2 presents the hydraulic geometry for both groups of data from Emmett's (1975) dataset analyzed by Eaton and Church (2007). The channel dimensions predicted by the CCV model fit to the data are shown as well. Because the channels are relatively small, vegetation plays an important role in conditioning the channel dimensions. Expressed as a dimensionless effective cohesion, C_r^*, the characteristic bank strength for the model fit to Group 1 is about 13, and for Group 2 it is about 20.

To illustrate the scale dependency of the effect of vegetation on boundary conditions, we have plotted the Q^*–S curves associated with the fitted models in Figure 2, using the Q^*–S equations predicted by the CRB equations for constant values of relative bank strength as a family of reference curves (Figure 3). In order to determine these curves, we fit a power function to the dimensionless widths and depths for Groups 1 and 2, together. The empirical equation [and a measure of the goodness-of-fit, the root mean square error (RMSE)] is:

$$W^* = 4{\cdot}04Q^{*0{\cdot}46} \text{ (RMSE = 15\%)} \tag{5}$$

Setting Equation 5 equal to Equation 2 and solving for S as a function of Q^* and μ' gives:

$$S = 0{\cdot}0954\mu'^{1{\cdot}83}Q^{*-0{\cdot}40} \tag{6}$$

In Figure 3, curves assuming $\mu' = 1$, 2 and 4 are plotted for reference. The Q^*–S curves for the CCV models clearly cut across

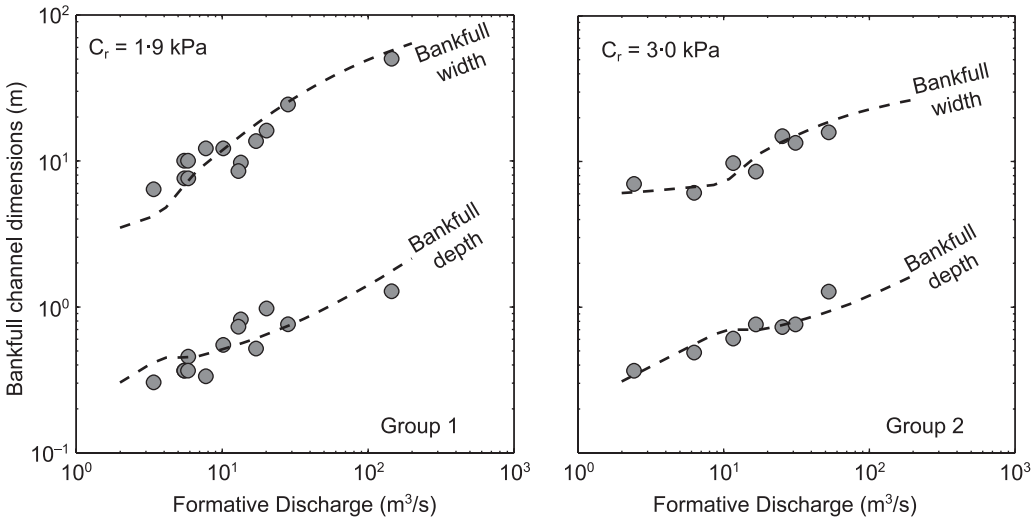

Figure 2. Salmon River CCV model fits (after Eaton and Church, 2007). The modeled widths and depths for Group 1 are shown, along with the measured channel dimensions reported by Emmett (1975), on the left hand panel. The results for Group 2 are on the right.

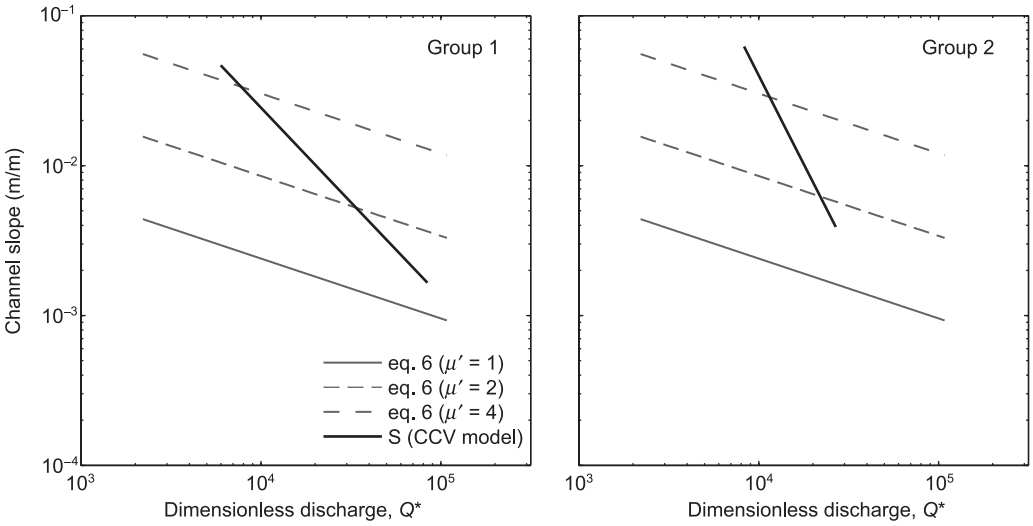

Figure 3. Q^*–S plots for models fit to data (after Eaton and Church, 2007) from the Salmon River area (Emmett, 1975). The results for Group 1 are on the left, and the results for Group 2 are on the right.

DOI: 10.1002/esp

these reference curves, ranging from relative bank strengths of about four (strong banks) for the smallest channels to values approaching one (banks as erodible as the bed) for the largest ones. It should be noted that S, D_{50} and Q were used to parameterize the CCV model, so we are really plotting the inputs that produce the model fits in Figure 2.

At some critical scale, the effect of vegetation on channel geometry becomes negligible, but that point depends on characteristic rooting depth of the riparian vegetation found on the floodplain, as well as the rate at which grain size, D_{50}, and channel gradient, S, decline downstream: it is because of these differences that the curves for Groups 1 and 2 are different. Nevertheless, the hydraulic geometry of these stream channels, which is typical of most channel networks, clearly implies that the relative bank strength for the system declines as the channel size increases, and that this systematic change is consistent with the assumptions built into the CCV model.

In the second part of the analysis of the scale effect of bank strength on downstream hydraulic geometry, the data published by Andrews (1984) are considered. These channels appear to have somewhat weaker banks (Eaton and Church, 2007). The dimensionless equations for channel width are:

$$W^* = 4{\cdot}94Q^{*0{\cdot}48} \text{ (RMSE 13\%) (thin vegetation)} \quad (7)$$

$$W^* = 3{\cdot}91Q^{*0{\cdot}48} \text{ (RMSE 8\%) (thick vegetation)} \quad (8)$$

In order to generate a unique Q^*–S function, a single power function was fitted to the widths for the entire Andrews (1984) dataset (shown in Figure 4). The dimensionless hydraulic geometry equation is:

$$W^* = 3{\cdot}37Q^{*0{\cdot}51} \quad (9)$$

Setting Equation 9 equal to Equation 2 and solving for S, we get:

$$S = 0{\cdot}0705\mu'^{1{\cdot}83}Q^{*-0{\cdot}31} \quad (10)$$

In Figure 4, we plot Equation 10 assuming $\mu' = 1{\cdot}0$ and $\mu' = 2{\cdot}0$. The data for channels with thin vegetation tends to plot near the threshold for $\mu' = 1{\cdot}0$. The smallest channels with thick vegetation tend to plot near the threshold assuming $\mu' = 2{\cdot}0$, while the largest ones plot closer to the $\mu' = 1{\cdot}0$ threshold, suggesting that the relative bank strength for the more densely vegetated channels declines systematically with increasing channel scale.

The curves for $C_r^* = 3{\cdot}33$ ($H \approx 0{\cdot}20$ m, based on the average D_{50} of 60 mm) and $1{\cdot}67$ ($H \approx 0{\cdot}10$ m) were determined numerically using the CCV model (Figure 4). The C_r^* values used in the model were chosen in order to produce curves that run through Andrews' data points: they are lines-of-comparison, not values assigned to either group [see Eaton and Church (2007) for an analysis of the most likely C_r and H values for the two groups].

To define the curves in Figure 4, the CCV model was run by varying S to produce the hydraulic geometry predicted by Equation 9, so the Q^*–S curves represent a true prediction by the CCV model. The Q^*–S curves predicted by the CCV model cut across the curves based on the CRB equations, just as they do for Emmett's dataset. Most of Andrews' (1984) data for channels classified as having 'thick' riparian vegetation plot close to the thresholds for $C_r^* = 3{\cdot}33$ and $1{\cdot}67$. Andrews' data from channels with 'thin' riparian vegetation systematically plot below the $C_r^* = 1{\cdot}67$ threshold, indicating that these channels do indeed have slightly weaker banks than the channels with thick riparian vegetation.

For Q^* greater than 10^4, the plotting positions for 'thin' and 'thick' channels overlap, suggesting that the effect of vegetation is limited beyond this scale. In comparison, analysis of the more densely vegetated Salmon River channels suggests that the effect of vegetation persists at this scale (up to $Q^* \sim 10^5$), presumably because they are more densely vegetated. For channel scales greater than about $Q^* = 10^5$, the effect of vegetation on bank strength should not be discernable.

In Figure 4, the CCV curves actually cross the $\mu' = 1{\cdot}0$ threshold. Since, as C_r^* approaches zero, the CCV model becomes identical to the regime model used by Millar (2005) to define the CRB equations (assuming $\mu' = 1{\cdot}0$), the fact that the CCV lines cross the $\mu' = 1{\cdot}0$ threshold does not represent a real difference. The disparity is an effect related primarily to the assumptions about flow resistance made in Millar's analysis: the CCV model uses flow resistance values estimated from field data while Millar's analysis related flow resistance to grain size using a flow resistance law.

The final dataset, from Pitlick and Cress's (2002) analysis of the Colorado River, provides an opportunity to test the assertion that vegetation has minimal effect on the geometry of large channels. Interestingly, their data define an unusual hydraulic geometry (Figure 5), in that width increases more slowly and

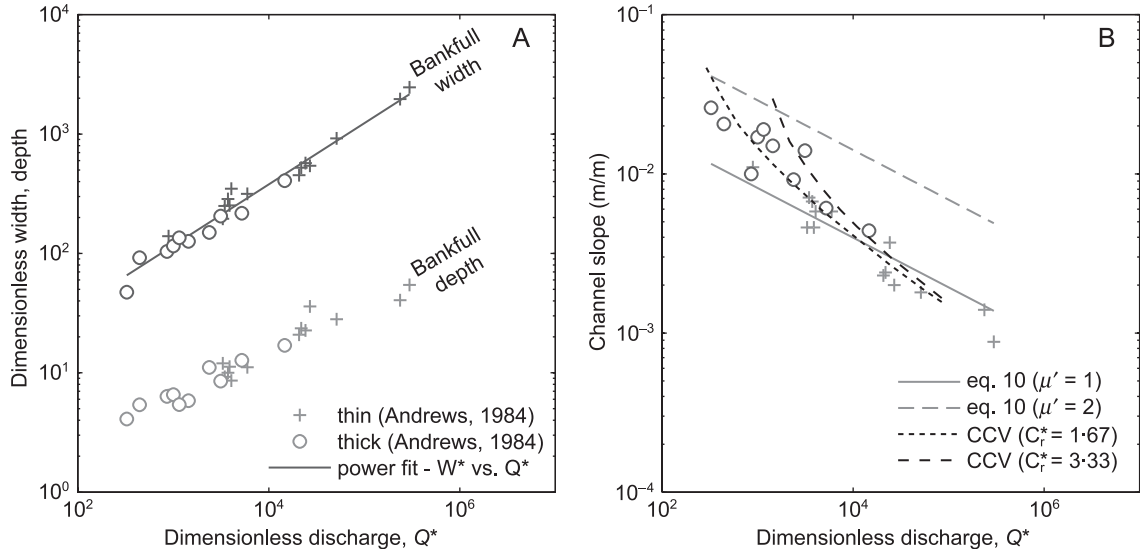

Figure 4. (A) Dimensionless hydraulic geometry data from Andrews (1984) are shown along with the power function for W^* used to derive Equation 10. (B) Q^*–S curves predicted by the CCV model and the CRB equations are compared with the data from Andrews (1984).

DOI: 10.1002/esp

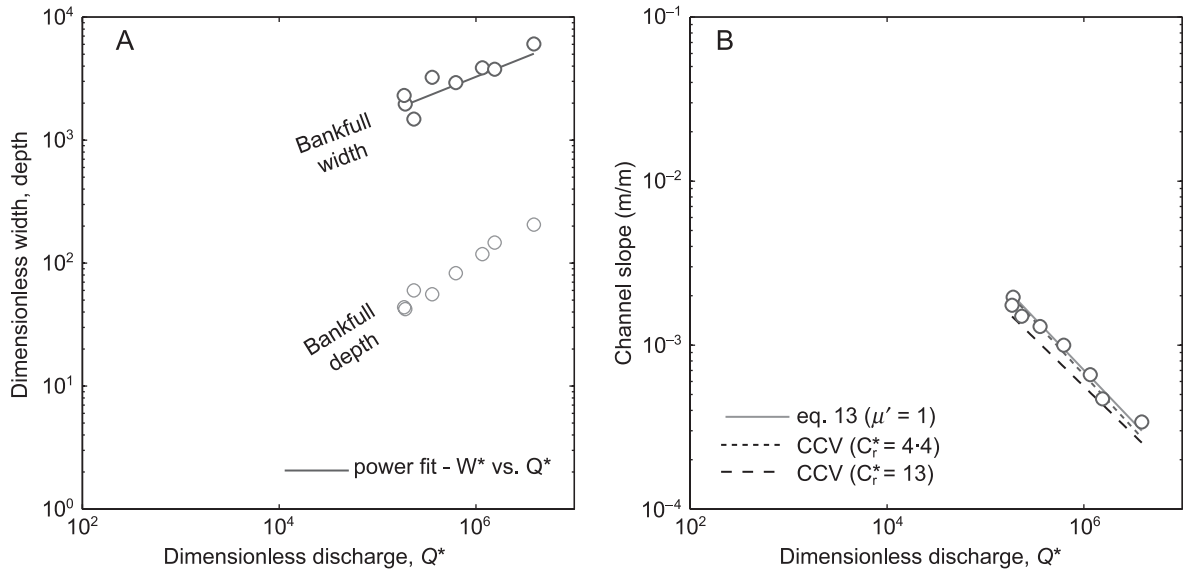

Figure 5. (A) Dimensionless hydraulic geometry data from Pitlick and Cress (2002) are shown along with their reported power function for W^*, which we used to derive Equation 13. (B) Q^*–S curves predicted by the CCV model and the CRB equations are compared with the data.

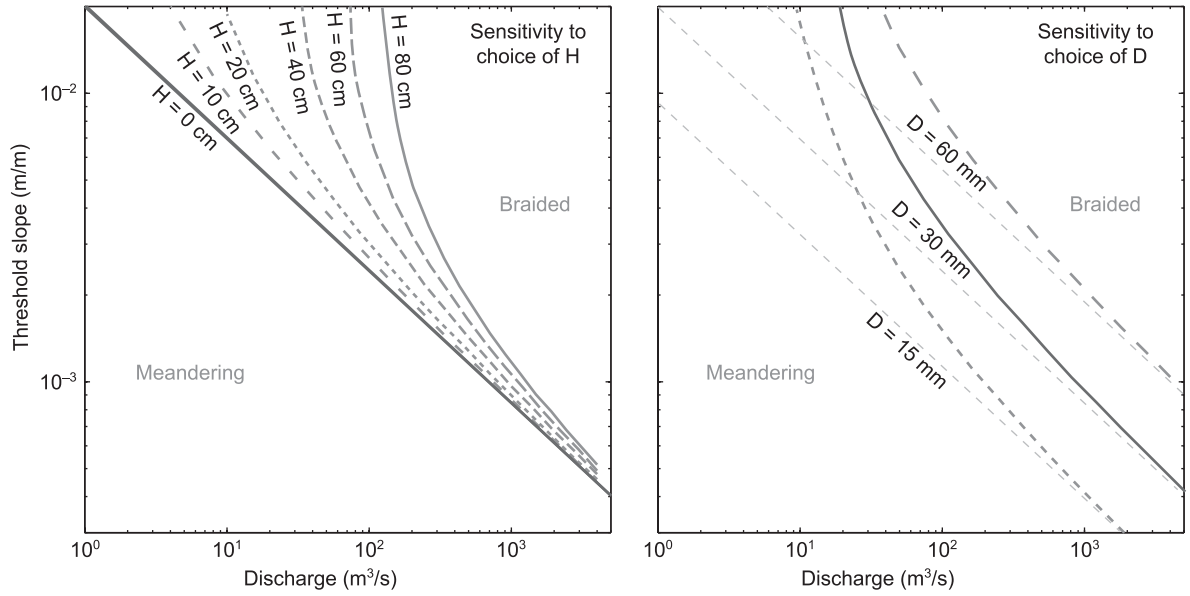

Figure 6. Meandering-braiding threshold slopes versus bankfull discharge as a function vegetation-related bank strength (H) and grain size (D). The left-hand side graph illustrates the numerically determined thresholds for D_{50} = 30 mm assuming H = 0, 10, 20, 40, 60 and 80 cm. On the right-hand side thresholds for D_{50} = 15, 30 and 60 mm are shown for H = 0 cm and H = 30 cm. The meandering and braided regions are labeled in gray.

depth more quickly than is expected based on the hydraulic geometry typically reported (Pitlick and Cress, 2002): Pitlick and Cress's dimensionless equations are:

$$W^* = 39{\cdot}3Q^{*0{\cdot}32} \text{ (RMSE 15\%)} \quad (11)$$

$$d^* = 0{\cdot}07Q^{*0{\cdot}53} \text{ (RMSE 9\%)} \quad (12)$$

Setting Equation 11 equal to Equation 2 gives us the Q^*–S curve associated with the CRB equations exhibiting the same hydraulic geometry:

$$S = 4{\cdot}25\mu'^{1{\cdot}83}Q^{*-0{\cdot}63} \quad (13)$$

Using the CCV model to replicate the hydraulic geometry expressed in Equation 11 assuming both a moderately high (C_r^* = 13) and low (C_r^* = 4·4) dimensionless cohesion yields curves that are almost indistinguishable from Equation 13 when μ' is set equal to unity. Based on the average D_{50} for this reach of the Colorado River (45 mm), C_r^* = 13 corresponds to H = 0·60 m, and C_r = 2·5 kPa, while C_r^* = 4·4 corresponds to H = 0·20 m and C_r = 0·80 kPa. A comparison between Equation 13 assuming μ' = 1 and the observed channel slopes shows a very close agreement between theory and field data (Figure 5). Since, for $Q^* > 10^5$, the CRB curve based on μ' = 1 and the CCV curves for C_r^* = 13 and 4·4 plot nearly on top of one another, it is reasonable to infer that riparian vegetation does not have a significant effect on the channel geometry for channels of this scale.

Meandering-braiding threshold

The following analysis uses the CCV model and a simplified version of Fredsoe's (1978) meandering-braiding criterion ($W/d \approx 50$). In the first set of analyses, the sensitivity of the numerically modeled braid threshold slope to the choice of D_{50} and H is assessed. The results are summarized in Figure 6. On the left-hand side, the results assuming D_{50} = 30 mm are

DOI: 10.1002/esp

presented: the threshold slope assuming no vegetation-related cohesion ($H = 0$ cm) is a power function, and represents the lowest threshold in the Q–S space. For increasingly stronger banks ($H = 10$–80 cm), the predicted threshold is displaced towards higher slopes, and becomes concave upwards.

When the grain size is doubled to 60 mm (H held constant at 0 cm and 30 cm) the thresholds are displaced upwards, as shown on the right-hand side of Figure 6. When the grain size is halved, the thresholds are displaced downwards. The shape of the curves in Q–S space also changes slightly, but the general structure remains unchanged. The degree to which the thresholds are shifted indicates that grain size has a larger effect on the threshold slope than H for channels at the large end of the discharge scale, but that for discharges equal to or less than about 100 m^3/s, H is at least as important as D_{50}.

Figure 7(A) presents the dimensionless thresholds relating the threshold slope to the dimensionless discharge, Q^* for various values of C_r^*. Thresholds associated with constant C_r^* but different H and D_{50} values plot upon the same dimensionless line. The collapse in Q^*–S space is due to the fact that changing D_{50} values produces a change in Q^* (Q held constant) effectively moving channels with smaller D_{50} farther 'downstream', in a dimensionless sense, and moving channels with larger D_{50} farther 'upstream'. The higher the value of C_r^*, the greater the degree of concavity in the Q^*–S curve for the threshold, and the steeper the slope upon which one can expect to find meandering channels. The equation for the curve assuming $C_r^* = 0$ can be derived using the CRB equations by forming the ratio of Equations 2 and 3, giving an equation for the W/d ratio, setting that equation equal to 50 and solving for S. The resulting equation is:

$$S = 0{\cdot}45\mu'^{1{\cdot}43}Q^{*-0{\cdot}44} \tag{14}$$

This function expresses the braiding threshold slope as a function of discharge, characteristic grain size and relative bank strength: power functions are shown in Figure 7(A) assuming $\mu' = 1$, 2 and 4. The curves for $C_r^* > 0$ asymptotically approach the curve assuming $\mu' = 1$, which is identical to the curve for $C_r^* = 0$. For the smallest channels, the C_r^* thresholds are consistent with Equation 14 if we assume that the banks are about two to four times as erosion resistant as is the bed for the smaller channels, but for the larger channels (i.e. $Q^* \sim 10^6$), the effect of vegetation has declined to the point that the thresholds are all equivalent to Equation 14 assuming $\mu' = 1$. Thus, when bank strength is attributable to riparian vegetation, the resistance of the boundary to erosion has a great effect on channel pattern for small single-thread channels, but this effect declines as the size of the channel under consideration increases. Beyond $Q^* \sim 10^6$, vegetation has an almost negligible effect on the meandering-braiding transition.

Data on braided gravel-bed channels from van den Berg (1995) are plotted in Figure 7(B). They are reasonably well bounded by the threshold assuming $C_r^* = 0$ (or equivalently, $\mu' = 1$). Similarly, meandering channels that are sparsely vegetated plot on or below the same threshold (shown in Figure 7C). However, for small channels that are more densely vegetated, many channels plot above the threshold, amongst the braided channels. Most plot below the braided threshold for $C_r^* = 6{\cdot}67$, and all but one plot below the threshold for $C_r^* = 13{\cdot}3$ (Figure 7D).

Densely vegetated channels with a single thread pattern are found in (but not above) the region between the meandering-

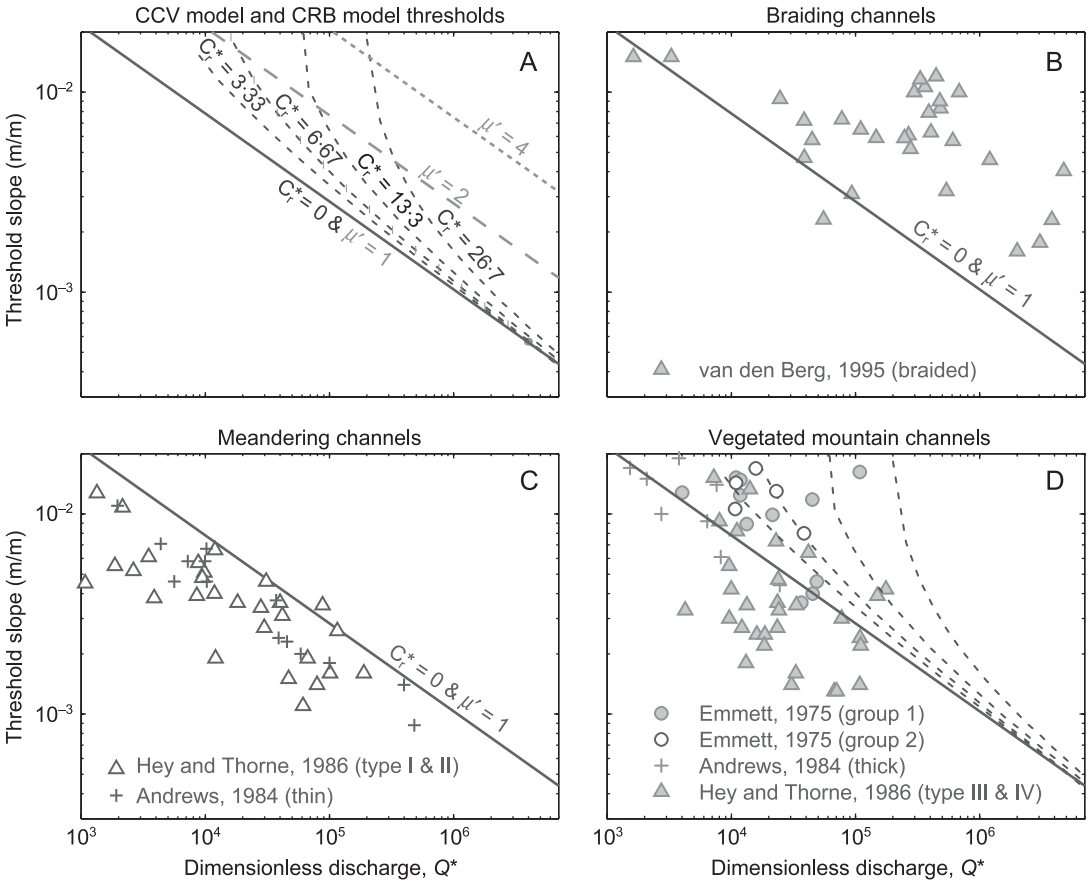

Figure 7. (A) Dimensionless meandering-braiding thresholds predicted by the CCV model and the CRB equations are compared. (B) Data from braiding channels is compared against the limit braiding threshold ($C_r^* = 0$, $\mu' = 1$). (C) Data from sparsely vegetated meandering channels is compared with the limit braiding threshold ($C_r^* = 0$, $\mu' = 1$). (D) Data from more densely vegetated single-thread channels are compared against the range of thresholds predicted by the CCV model (shown and labeled in A) assuming a range of reasonable bank strength parameters.

DOI: 10.1002/esp

Table I. Coefficients and model statistics for fitted models[a] relating μ' to Q^* for constant C_r^*

C_r^*	p_1	q_1	q_2	q_3	Adj. R^2	RMSE	SSE
26·67	4·567	–19·33	125·5	–269·8	0·9992	0·01221	0·001491
20·00	4·417	–18·61	116·3	–240·0	0·9987	0·01862	0·003122
13·33	9·115	–18·39	114·2	–231·2	0·9995	0·007908	0·0005002
10·00	10·05	–17·72	106·2	–206·1	0·9996	0·007802	0·0004261
6·66	13·64	–17·08	99·06	–182·7	0·9995	0·007783	0·000424
3·33	18·53	–15·57	83·15	–135·4	0·9987	0·006723	0·000226

[a] The model is: $\mu' = p_1/[(\log(Q^*)^3 + q_1\log(Q^*)^2 + q_2\log(Q^*) + q_3)]$.

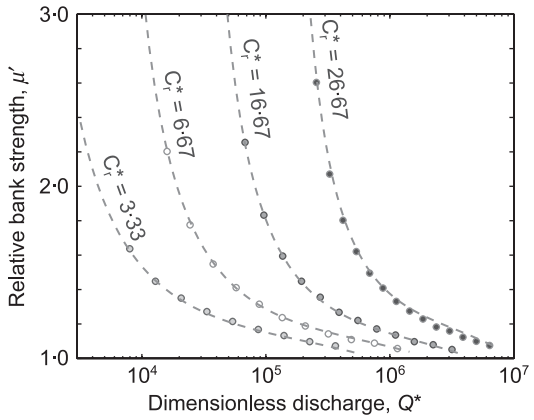

Figure 8. Relation between relative bank strength (μ') and dimensionless discharge for constant values of C_r^*. The circles represent the points at which μ' was determined numerically, and the dashed lines represent equations fit to the data (see Table I).

braiding thresholds assuming $C_r^* = 0$ and $C_r^* = 26{\cdot}7$, and sparsely vegetated channels are not found there, confirming the prediction of the theory. More generally, the model predicts that channels falling between the curves $C_r^* = 0$ and $C_r^* = 26{\cdot}7$ have patterns that are significantly influenced by the role that vegetation plays in strengthening the channel banks as suggested by Millar (2000). Unlike Millar's analysis, this analysis clearly indicates that the effect is strongly scale dependent, disappearing for $Q^* > 10^6$ (if $D_{50} = 30$ mm, this corresponds to $Q \approx 600$ m^3/s).

In order to produce usable mathematical forms of the threshold equations shown in Figure 7(A) we first mapped the values of μ' to Q^* for the curves for constant C_r^*, since if we can determine the value of μ' that corresponds to each coordinate (C_r^*, Q^*), then the critical slope can be calculated using Equation 14. In order to do this, we calculated μ' by substituting the solution values of S and Q^* from the C_r^* models into Equation 14 and then solving for μ'. The results are expressed as functions relating μ' to Q^* for given values of C_r^*, as shown in Figure 8. Relative bank strength declines with Q^* for all values of C_r^*, but the rate of decline varies. Empirical functions have been fit to the data in Figure 8; they are presented Table I and shown on Figure 8 as dashed lines.

Threshold for channel migration

While the analyses of downstream hydraulic geometry and the meandering-braiding transition demonstrate that the effect of vegetation on bank strength declines as channel scale increases and effectively disappears for $Q^* > 10^6$, recent work from the Pacific Northwest suggests the existence of a point at the other end of the spectrum below which vegetation dominates the channel dynamics to such a degree that lateral channel migration is severely constrained (Beechie *et al.*, 2006). Beechie *et al.* associated this threshold with channels for which depth, d, is approximately equal to the rooting depth, H, of the riparian species. The CCV model is ideally parameterized to investigate this threshold.

This was done by using the CCV model to find combinations of H and Q for which the total channel depth, d, is nearly equal to H. The range of H was specified based on the analysis of Hey and Thorne's (1986) dataset by Eaton (2006) using the CCV model: the results of that analysis imply that H values range from about 0·30 m for the most sparsely vegetated channels (Hey and Thorne's type I), up to about 1·0 m for the most densely vegetated ones (type IV). Figure 9(A) presents the channel migration threshold discharge predicted by the CCV model for the specified range of rooting depths. Two curves are presented, representing model predictions for two different characteristic grain sizes (D_{50} = 30 mm and 45 mm). The threshold discharge for channel migration increases with H, ranging from close to 2 m^3/s for type I channels to around 40 m^3/s for type IV channels. In Figure 9(B), the widths associated with the threshold discharge are also plotted against H, so that they may be compared with the critical widths reported by Beechie *et al.* (2006). The critical widths predicted by the CCV model range from about 5 m for type I channels to about 25 m for type IV channels.

Power functions (also shown on Figure 9) were used to relate the critical discharge (as well as the associated width) to H. By expanding the range of grain sizes for which the critical discharges and widths were calculated to 24–64 mm, general forms of the threshold equations were numerically determined. The general form, with all quantities in standard SI units, is given by:

$$Q_{crit} = F_{D_{50}} H^{2{\cdot}0}, \text{ where } F_{D_{50}} = 4{\cdot}0(D_{50})^{-0{\cdot}70} \quad (15)$$

$$W_{crit} = G_{D_{50}} H^{0{\cdot}88}, \text{ where } G_{D_{50}} = 1{\cdot}4(D_{50})^{-0{\cdot}86} \quad (16)$$

A comparison between these equations and Beechie *et al.*'s (2006) empirical findings supports our theoretical analysis. The characteristic rooting depths for riparian vegetation around the coastal stream channel in the Pacific Northwest studied by Beechie *et al.* is between 0·5 m and 0·75 m. Assuming D_{50} = 30 mm, Equation 16 predicts that the width threshold for lateral migration should be between 16 m and 22 m: Equation 15 predicts that the discharge threshold should be between 12 m^3/s and 26 m^3/s. Assuming D_{50} = 45 mm, the equations predict critical widths ranging from 11 m to 16 m and critical discharges ranging from 9 m^3/s to 20 m^3/s. Both sets of calculations compare favorably with the range of critical widths (15 m to 20 m) reported by Beechie *et al.* (2006) and with their reported critical discharge (15 m^3/s).

These threshold equations can also be applied to understand the behavior documented at Fishtrap Creek following a forest fire in 2003. Fishtrap Creek is more sparsely vegetated than

DOI: 10.1002/esp

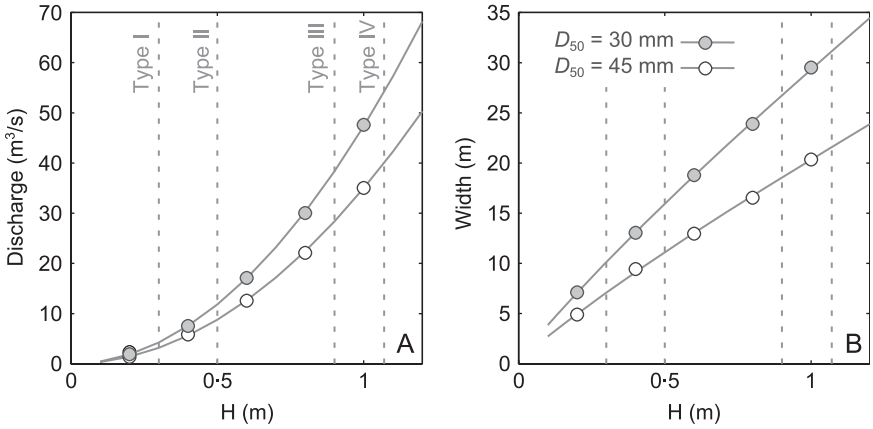

Figure 9. Channel migration threshold as a function of the characteristic rooting depth for riparian vegetation. (A) The threshold discharge for the D_{50} = 30 mm (filled circles) and D_{50} = 45 mm (open circles) is plotted against H. (B) The threshold width is plotted. The characteristic H value estimated for Hey and Thorne's (1986) four riparian vegetation types are indicated on both figures by vertical dashed lines.

Figure 10. (A) and (B) show photographs taken from approximately the same location in Fishtrap Creek, illustrating the change in channel morphology from plane bed to riffle-pool morphology; (C) and (E) show an area where rapid channel widening occurred during the 2007 freshet; (D) shows an eroding bank, as well as some of the remaining large roots: the smaller roots appear have rotted away. The approximate depth to which the root systems originally extended is indicated in photograph D. The locations labeled 'former channel width' in photographs C and E indicate the approximate channel dimensions at the beginning of the 2007 spring freshet. The changes in channel width occurred over a period of about two days. This figure is available in colour online at www.interscience.wiley.com/journal/espl

the coastal streams studied by Beechie *et al*. (2006). Prior to the fire, the floodplain of Fishtrap Creek had a vegetation cover dominated by cottonwoods and red cedar. The stream channel appeared to have been stable for many years prior to the fire, and continued to remain laterally stable for two to three years after the fire (Figure 10A). The typical channel morphology during this stable phase was a gravel plane bed type (after Montgomery and Buffington, 1997). Beginning during the snowmelt freshet in 2006 and continuing throughout the freshet of 2007, the channel has widened (and in some places aggraded) and the morphology has shifted to something closer to a riffle-pool type (Figure 10B).

Based on Water Survey of Canada gauging records at the study site, the mean annual peak flow for Fishtrap Creek is about 7·4 m^3/s: since the forest fire in 2003, the annual peaks have reached 4·6, 8·9, 7·2 and 6·6 m^3/s in 2004, 2005, 2006, and 2007, respectively. The suspended sediment supply from the hillslopes was similarly unaffected by the fire (Petticrew

DOI: 10.1002/esp

et al., 2006). The typical rooting depth for the riparian tree species, as determined by examining cutbanks along the stream channel, appears to have been on the order of 50 cm, prior to the fire, but the smaller roots rapidly decayed after the fire and the banks quickly lost strength. In 2007, only the upper 10 cm to 20 cm were being effectively stabilized by the grasses that had colonized the floodplain (Figure 10D). The surface D_{50} averaged about 50 mm throughout the reach. Using $H = 50$ cm and $D_{50} = 50$ mm in Equations (15) and (16) predicts a critical width of 8·1 m and a critical discharge of 10 m^3/s. So, with an intact riparian forest, Fishtrap Creek would fall almost directly upon the lateral migration threshold and should not migrate laterally, which appears to have been the case for the pre-fire stream channel.

Significant channel change first occurred in 2006 in response to a peak flow of only 7·2 m^3/s. Much more widespread erosion occurred in 2007, when the channel nearly doubled its width in some locations (Figures 10C and 10E), this time in response to a peak flow of 6·6 m^3/s. If we assume that the effective rooting depth had dropped from around 50 cm to about 20 cm by 2007, then the critical discharge predicted by Equation 15 drops from 11 m^3/s to 5·0 m^3/s. Both the model and the field observations suggest that channels like Fishtrap Creek are laterally stable when forested, at which time the typical channel morphology seems to be the relatively featureless plane bed type (Figure 10A). Once the strength of the dead root systems decayed sufficiently, the channel became laterally active and adopted something more like a typical riffle-pool morphology (Figure 10B).

Discussion and Conclusions

The analysis of downstream hydraulic geometry using the CCV model clearly demonstrates that the effect of vegetation on bank erodibility (and hence channel geometry) is significant for small streams, but that it declines as channel size increases. This scale effect is a likely explanation for the common observation that *W/d* ratios typically increase downstream. If the boundary shear stress remains about the same, relative to the characteristic grain size for the system (i.e. the dimensionless shear stress is constant), then increases in the bankfull *W/d* ratio are predicted to be the result of declining relative bank strength (Eaton *et al.*, 2004). Furthermore, beyond the scale at which the effects of vegetation on bank strength disappear, which the analysis indicates is around $Q^* = 10^4$ to 10^5, we should not expect the characteristic increase in *W/d* with *Q* to occur. Pitlick and Cress's (2002) dataset is restricted to channels for which $Q^* > 10^5$, and their data imply that *W/d* ratios decline with channel scale, in contrast to the typically observed downstream increase in *W/d*.

Interestingly, datasets describing the bankfull characteristics of channel anabranches (Tabata and Hickin, 2003; Ellis and Church, 2005) show a very rapid increase in *W/d* ratio with the discharge carried by each anabranch channel. Those unusual hydraulic geometries can be attributed to the fact that neither slope nor grain size vary systematically with discharge (Eaton and Church, 2007), which is not the case in true downstream hydraulic geometry relations. So, while the scale dependency of vegetation-related bank strength is clearly not the only reason that *W/d* ratios might be expected to increase with *Q*, it is probably an important factor, especially for datasets that include small channels with densely vegetated floodplains.

This scale effect, hidden as it is within the empirical hydraulic geometry equations such as those reported by Emmett (1975), has implications for the way in which empirical hydraulic geometry equations are used. Hydraulic geometry equations that account for riparian vegetation (e.g. Andrews, 1982; Hey and Thorne, 1986) are strictly limited with respect to the range of scales over which they can reasonably be applied. Clearly, for large systems (i.e. $Q^* > 10^5$) it is unlikely that riparian vegetation will significantly affect channel geometry, and all channels will probably conform to the geometry predicted by the equation for sparse riparian vegetation. Similarly, if the equations are applied to channels smaller than those in the datasets from which the equations were derived, it is quite likely that the relative bank strength will be greater than expected, and the predicted channel *W/d* ratio will be greater than observed. Our analysis suggests that for channels with $Q^* < 10^5$, we should expect different relations for different characteristic riparian vegetation types and densities, all of which will probably exhibit an increase in *W/d* with channel scale. For $Q^* > 10^6$, we should expect little or no vegetation-related effect on the hydraulic geometry. These channels may exhibit *W/d* ratios that either increase or decrease with discharge (or remain the same), but these changes are likely to be driven by the variations in grain size and channel slope, as suggested by Pitlick and Cress (2002), not by vegetation.

Fitting a single hydraulic geometry equation to channels from both above and below $Q^* = 10^6$ is probably misleading, since this fails to acknowledge both the role vegetation plays in controlling channel geometry and the limit scale for this effect, beyond which the effect is negligible. Fitting power functions to the data from channels where the effect of vegetation is particularly strong (such as the Salmon River data in Figure 2) is probably not appropriate, since the relative bank strength changes rapidly enough to produce trends that change more quickly than predicted by power functions.

When empirical hydraulic geometry equations are used to specify the channel network characteristics in landscape evolution models (e.g. Tucker and Bras, 1998), and thereby calculate the sediment transport capacity of the channel system, the variations in bank strength, grain size and slope with discharge that are intrinsic to the empirical equations are also included. This may be undesirable, particularly when the model purports to describe the effect of vegetation on landscape development (e.g. Istanbulluoglu and Bras, 2005). Such models could be improved by employing the physically based hydraulic geometry equations presented by Millar (2005) and developing some reasonable function that depends on vegetation type and scale to determine (and vary) the relative bank strength (μ') used in those equations.

Similarly, the effect of vegetation on the meandering-braiding transition is strongest for the smallest values of Q^*, and diminishes as Q^* increases. While all of the sparsely vegetated channels in Figure 7(C) are found at or below the Q^*–S threshold assuming no vegetation-related bank strength and all of the braided channels in Figure 7(B) are found at or above the threshold, channels for which vegetation does affect bank strength are found on either side of it (Figure 7D). None of the channels in Figure 7(D) are found above the threshold for a dimensionless effective cohesion, C_r^*, of 26·7, and only four of the are found above the curve for $C_r^* = 6{\cdot}67$, suggesting that these may represent more realistic braiding thresholds for streams with densely vegetated floodplains. For a gravel-bed stream having $D_{50} = 45$ mm, $C_r^* = 6{\cdot}67$ corresponds to a rooting depth, H, of 0·3 m and an average root cohesion, C_r, for the upper bank of about 1·3 kPa, values that are characteristic of Hey and Thorne's (1986) most sparsely vegetated channels; $C_r^* = 26{\cdot}7$ corresponds to $H = 1{\cdot}2$ m and $C_r = 5$ kPa, characteristic of a very densely forested floodplain with particularly deep-rooted riparian vegetation. The zone between the curve for $C_r^* = 26{\cdot}7$ and $C_r^* = 0$ represents the

DOI: 10.1002/esp

region in which channel morphology is potentially controlled by riparian vegetation, since channels can either adopt a meandering pattern or a braided one, depending on the density of the riparian vegetation and the strength of the channel banks.

At the other end of the scale, vegetation can so dominate channel dynamics that lateral migration becomes insignificant. Beechie *et al*. (2006) set this threshold at a bankfull discharge of about 15 m^3/s, and suggest that this is the discharge at which rooting depth and bank height are approximately equal. Modeling using the CCV model suggests that this empirical observation is consistent with regime theory. Furthermore, regime theory is capable of predicting the relation between the threshold discharge and the rooting depth, as shown in Figure 9. Evidence from Fishtrap Creek, which has less dense riparian vegetation than Beechie *et al.*'s streams, suggests that the threshold for lateral migration is closer to 10 m^3/s. Once the riparian root systems at this site were destroyed by a forest fire, the bank strength fell and the channel began to erode its banks and to migrate laterally. Channel morphology appears to have shifted from a plane bed morphology to a riffle-pool morphology as a result (Figures 10A and 10B). This suggests that two conclusions can be made about channel migration: (1) the threshold discharge is a function of the riparian vegetation, and changes as the riparian community is disturbed (and recovers); (2) changes in the riparian vegetation can provoke changes in channel morphology if the changes drive the fluvial system across the lateral migration threshold. These sorts of changes need not be associated with increases in the sediment supply from upstream nor with increases in the peak flows; morphologic change in this case can be a purely endogenous process, as appears to be the case at Fishtrap Creek.

These analyses of the channel migration threshold suggest that channels in humid regions where floodplains typically support continuous covers of trees and/or shrubs are likely to reflect some aspects of the disturbance regime that affects the riparian vegetation. These effects will be most pronounced for channels having bankfull discharges between 5 m^3/s and possibly as much as 50 m^3/s. Channels of this scale may experience periods of significantly reduced lateral activity when riparian trees are able to render the channel banks nearly non-erodible. During these periods of stability, these channels may evolve relatively featureless morphologies with few bars and only poorly developed pools. Periods of relatively intense lateral migration, accompanied by the development of riffle-pool features, are likely to occur once the riparian vegetation is disturbed.

In regions like the interior of British Columbia, where forest fires recur approximately every 100 years, this shift between laterally active riffle pool systems and laterally stable plane bed channels may occur quite frequently. In such environments, the disturbance due to fire may be an essential component of maintaining a diverse physical habitat for the aquatic ecosystems. In fact, for those channels that are close to the lateral migration threshold, the concept of a dynamic steady state with respect to the supply of water and sediment may not be as useful as the concept of a relatively continuous oscillation between channel states associated with the disturbance and recovery of the riparian vegetation. Channel morphology for these channels, then, would be best interpreted as an indicator of the position in the evolutionary cycle driven by the forest fire disturbance regime, rather than reflections of disturbances occurring upstream.

Acknowledgements—This work was supported by grants from the Natural Sciences and Engineering Research Council of Canada and from the British Columbia Forest Sciences Program. Early discussions with Rob Millar (University of British Columbia) and Ed Johnson (University of Calgary) helped shape the analysis. The detailed and constructive comments of two anonymous reviewers greatly improved the paper: their efforts are greatly appreciated.

References

Abernethy B, Rutherfurd ID. 1998. Where along a river's length will vegetation most effectively stabilise stream banks. *Geomorphology* **23**: 55–75.

Andrews ED. 1982. Bank stability and channel width adjustment, East Fork River, Wyoming. *Water Resources Research* **18**(4): 1184–1192.

Andrews ED. 1984. Bed material entrainment and the hydraulic geometry of gravel-bed rivers in Colorado. *Geological Society of America Bulletin* **95**(3): 371–378.

Beechie TJ, Liermann M, Pollock MM, Baker S, Davies J. 2006. Channel pattern and river-floodplain dynamics in forested mountain river systems. *Geomorphology* **78**: 124–141.

Brooks AP, Brierley GJ, Millar RG. 2003. The long-term control of vegetation and woody debris on channel and flood-plain evolution: insights from a paired catchment study in southeastern Australia. *Geomorphology* **51**(1–3): 7–29.

Brooks GR. 2003. Holocene lateral channel migration and incision of the Red River, Manitoba, Canada. *Geomorphology* **54**(3–4): 197–215.

Buffington JM, Montgomery DR. 1999. Effects of sediment supply on surface textures of gravel-bed rivers. *Water Resources Research* **35**(11): 3523–3530.

Carson MA. 1984. The meandering – braided river threshold: a reappraisal. *Journal of Hydrology* **73**: 315–334.

Carson MA, Kirkby MJ. 1972. *Hillslope Form and Process*. Cambridge University Press: London; 475 pp.

Chang HH. 1979. Minimum stream power and river channel patterns. *Journal of Hydrology* **41**: 303–327.

Church M. 1995. Geomorphic response to river flow regulation: case studies and time-scales. *Regulated Rivers Research and Management* **11**: 3–22.

Church M. 2006. Bed material transport and the morphology of alluvial river channels. *Annual Review of Earth and Planetary Science* **34**: 325–354.

Church M, Hassan MA. 2002. Mobility of bed material in Harris Creek. *Water Resources Research* **38**(11): 1237. DOI: 10.1029/2001WR000753

Church M, Hassan MA, Wolcott JF. 1998. Stabilizing self-organized structures in gravel-bed stream channels: field and experimental observations. *Water Resources Research* **34**(11): 3169–3179.

Dade WB. 2000. Grain size, sediment transport and alluvial channel pattern. *Geomorphology* **35**(1–2): 119–126.

Davies TRH, Sutherland AJ. 1983. Extremal hypotheses for river behavior. *Water Resources Research* **19**(1): 141–148.

Dietrich WE, Kirchner JW, Ikeda H, Iseya F. 1989. Sediment supply and the development of the coarse surface layer in gravel-bedded rivers. *Nature* **340**: 215–217.

Eaton BC. 2006. Bank stability analysis for regime models of vegetated gravel bed rivers. *Earth Surface Processes and Landforms* **31**: 1438–1444.

Eaton BC, Church M. 2007. Predicting downstream hydraulic geometry: a test of rational regime theory. *Journal of Geophysical Research* **112**: F03025. DOI: 10.1029/2006JF000734

Eaton BC, Millar RG. 2004. Optimal alluvial channel width under a bank stability constraint. *Geomorphology* **62**: 35–45.

Eaton BC, Church M, Davies TRH. 2006. A conceptual model for meander initiation in bedload-dominated streams. *Earth Surface Processes and Landforms* **31**: 875–891.

Eaton BC, Church M, Millar RG. 2004. Rational regime model of alluvial channel morphology and response. *Earth Surface Processes and Landforms* **29**(4): 511–529.

Ellis ER, Church M. 2005. Hydraulic geometry of secondary channels of lower Fraser River, British Columbia, from acoustic doppler profiling. *Water Resources Research* **41**: W08421. DOI: 10.1029/2004WR003777

Emmett WW. 1975. *The Channels and Waters of the Upper Salmon River Area, Idaho*, US Geological Survey Professional Paper 870-A. US Geological Survey: Reston, VA.

Fredsoe J. 1978. Meandering and braiding of rivers. *Journal of Fluid Mechanics* **84**(4): 609–624.

Friedkin JF. 1945. *A Laboratory Study of the Meandering of Alluvial Rivers*. US Waterways Engineering Experimental Station: Vicksberg.

Friedman JM, Osterkamp WR, Lewis WMJ. 1996. Channel narrowing and vegetation development following a Great Plains flood. *Ecology* **77**(7): 2167–2181.

Gaeuman D, Schmidt JC, Wilcock PR. 2005. Complex channel responses to changes in stream flow and sediment supply on the lower Duchesne River, Utah. *Geomorphology* **64**(3–4): 185–206.

Gran K, Paola C. 2001. Riparian vegetation controls on braided stream dynamics. *Water Resources Research* **37**(12): 3275–3283.

Hey RD, Thorne CR. 1986. Stable channels with mobile gravel beds. *Journal of the Hydraulics Division-ASCE* **112**(8): 671–689.

Hickin EJ. 1984. Vegetation and river channel dynamics. *Canadian Geographer* **28**(2): 111–123.

Huang HQ, Nanson GC. 1998. The influence of bank strength on channel geometry: an integrated analysis of some observations. *Earth Surface Processes and Landforms* **23**: 865–876.

Huang HQ, Chang HH, Nanson GC. 2004. Minimum energy as the general form of critical flow and maximum flow efficiency and for explaining variations in river channel pattern. *Water Resources Research* **40**: W04502. DOI: 10.1029/2003WR002539

Hupp CR, Osterkamp WR. 1996. Riparian vegetation and fluvial geomorphic processes. *Geomorphology* **14**: 277–295.

Istanbulluoglu E, Bras RL. 2005. Vegetation-modulated landscape evolution: effects of vegetation on landscape processes, drainage density, and topography. *Journal of Geophysical Research* **110**: F02012. DOI: 10.1029/2004JF000249

Jeffries R, Darby SE, Sear DA. 2003. The influence of vegetation and organic debris on flood-plain sediment dynamics: case study of a low-order stream in the New Forest, England. *Geomorphology* **51**(1–3): 61–80.

Kirkby MJ. 1977. Maximum sediment efficiency as a criterion for alluvial channels. In *River Channel Changes*, Gregory KJ (ed.). John Wiley & Sons: Chichester; 429–442.

Leopold LB, Wolman MG. 1957. *River Channel Patterns; Braided Meandering and Straight*, US Geological Survey Professional Paper 282-B. US Geological Survey: Reston, VA.

Lisle TE, Church M. 2002. Sediment transport-storage relations for degrading, gravel bed channels. *Water Resources Research* **38**(11): 1219. DOI: 10.1029/2001WR001086

Millar RG. 2000. Influence of bank vegetation on alluvial channel patterns. *Water Resources Research* **36**(4): 1109–1118.

Millar RG. 2005. Theoretical regime equations for mobile gravel-bed rivers with stable banks. *Geomorphology* **64**: 207–220.

Millar RG, Quick MC. 1993. Effect of bank stability on geometry of gravel rivers. *Journal of Hydraulic Engineering-ASCE* **119**(12): 1343–1363.

Millar RG, Quick MC. 1998. Stable width and depth of gravel-bed rivers with cohesive banks. *Journal of Hydraulic Engineering-ASCE* **124**(10): 1005–1013.

Montgomery DR, Buffington JM. 1997. Channel-reach morphology in mountain drainage basins. *Geological Society of America Bulletin* **109**(5): 596–611.

Murray AB, Paola C. 2003. Modelling the effect of vegetation on channel pattern in bedload rivers. *Earth Surface Processes and Landforms* **28**(2): 131–143.

Nanson GC, Knighton AD. 1996. Anabranching rivers: their cause, character and classification. *Earth Surface Processes and Landforms* **21**: 217–239.

Owens PN, Blake WH, Petticrew EL. 2006. Changes in sediment sources following wildfire in mountainous terrain: a paired-catchment approach, British Columbia, Canada. *Water, Air, and Soil Pollution: Focus* **6**: 637–645.

Parker G. 1979. Hydraulic geometry of active gravel rivers. *Journal of Hydraulics Division – ASCE* **105**: 1185–1201.

Parker G, Klingeman PC. 1982. On why gravel bed rivers are paved. *Water Resources Research* **18**(5): 1409–1423.

Petticrew EL, Owens PN, Giles TR. 2006. Wildfire effects on the quality and composition of suspended and gravel-stored sediments. *Water, Air, and Soil Pollution: Focus* **6**: 647–656.

Pitlick J, Cress R. 2002. Downstream changes in the channel geometry of a large gravel bed river. *Water Resources Research* **38**(10): 1216. DOI: 10.1029/2001WR000898

Pollen N, Simon A. 2005. Estimating the mechanical effects of riparian vegetation on stream bank stability using a fiber bundle model. *Water Resources Research* **41**: W07025. DOI: 10.1029/2004WR003801

Pollen-Bankhead N, Simon A. 2008. Enhanced application of root-reinforcement algorithms for bank-stability modeling. *Earth Surface Processes and Landforms*. DOI: 10.1002/esp.1690

Reid I, Frostick LE, Brayshaw AC. 1992. Microform roughness elements and the selective entrainment and entrapment of particles in gravel-bed rivers. In *Dynamics of Gravel-bed Rivers*, Billi P, Hey RD, Thorne CR, Tacconi P (eds). John Wiley & Sons: Chichester; 253–265.

Rowntree KM, Dollar ESJ. 1999. Vegetation controls on channel stability in the Bell River, Eastern Cape, South Africa. *Earth Surface Processes and Landforms* **24**: 127–134.

Simon A, Collison AJC. 2002. Quantifying the mechanical and hydrologic effects of riparian vegetation on streambank stability. *Earth Surface Processes and Landforms* **27**(5): 527–546.

Simpson CJ, Smith DG. 2001. The braided Milk River, northern Montana, fails the Leopold–Wolman discharge-gradient test. *Geomorphology* **41**: 337–353.

Tabata KK, Hickin EJ. 2003. Interchannel hydraulic geometry and hydraulic efficiency of the anastomosing Columbia River, southeastern British Columbia, Canada. *Earth Surface Processes and Landforms* **28**: 837–852.

Tal M, Paola C. 2007. Dynamic single-thread channels maintained by the interaction of flow and vegetation. *Geology* **35**(4): 347–350.

Tal M, Gran K, Murray AB, Paola C, Hicks DM. 2004. Riparian vegetation as a primary control on channel characteristics in multi-thread rivers. In *Hydraulic, Hydrologic, and Geotechnical Interactions*, Bennett SJ, Simon A (eds). Water Science and Application, American Geophysical Union: Washington, DC. DOI: 10.1029/008WS04

Tribe S, Church M. 1999. Simulations of cobble structure on a gravel streambed. *Water Resources Research* **35**(1): 311–318.

Tucker GE, Bras RL. 1998. Hillslope processes, drainage density, and landscape morphology. *Water Resources Research* **30**(10): 2751–2764.

Van den Berg JH. 1995. Prediction of alluvial channel pattern of perennial rivers. *Geomorphology* **12**: 259–279.

Van de Wiel MJ, Darby SE. 2007. A new model to analyse the impact of woody riparian vegetation on the geotechnical stability of riverbanks. *Earth Surface Processes and Landforms* **32**: 2185–2198.

White WR, Bettess R, Paris E. 1982. Analytical approach to river regime. *Journal of the Hydraulics Division-ASCE* **108**(HY10): 1179–1193.

Wilcock PR, McArdell BW. 1993. Surface-based fractional transport rates: mobilization thresholds and partial transport of a sand-gravel sediment. *Water Resources Research* **29**(4): 1297–1312.